
This is an electronic reprint of the original article.
This reprint may differ from the original in pagination and typographic detail.

Caroppi, Gerardo; Västilä, Kaisa; Gualtieri, Paola; Järvelä, Juha; Giugni, Maurizio; Rowiński, Paweł M.

Comparison of Flexible and Rigid Vegetation Induced Shear Layers in Partly Vegetated Channels

Published in:
Water Resources Research

DOI:
[10.1029/2020WR028243](https://doi.org/10.1029/2020WR028243)

Published: 01/03/2021

Document Version
Publisher's PDF, also known as Version of record

Published under the following license:
CC BY

Please cite the original version:
Caroppi, G., Västilä, K., Gualtieri, P., Järvelä, J., Giugni, M., & Rowiński, P. M. (2021). Comparison of Flexible and Rigid Vegetation Induced Shear Layers in Partly Vegetated Channels. *Water Resources Research*, 57(3), Article e2020WR028243. <https://doi.org/10.1029/2020WR028243>

This material is protected by copyright and other intellectual property rights, and duplication or sale of all or part of any of the repository collections is not permitted, except that material may be duplicated by you for your research use or educational purposes in electronic or print form. You must obtain permission for any other use. Electronic or print copies may not be offered, whether for sale or otherwise to anyone who is not an authorised user.

Water Resources Research

RESEARCH ARTICLE

10.1029/2020WR028243

Key Points:

- Dynamically similar shear layers shared analogous lateral distributions of flow velocity and derived quantities
- Higher shear penetration within the vegetation was observed for flexible foliated plants in comparison to rigid cylinders
- Vegetation morphology and flexibility were found to affect key exchange processes across the vegetated interface

Supporting Information:

- Supporting Information S1

Correspondence to:

G. Caroppi,
gerardo.caroppi@aalto.fi

Citation:

Caroppi, G., Västilä, K., Gualtieri, P., Järvelä, J., Giugni, M., & Rowiński, P. M. (2021). Comparison of flexible and rigid vegetation induced shear layers in partly vegetated channels. *Water Resources Research*, 57, e2020WR028243. <https://doi.org/10.1029/2020WR028243>

Received 25 JUN 2020

Accepted 6 FEB 2021

© 2021. The Authors.

This is an open access article under the terms of the [Creative Commons Attribution License](#), which permits use, distribution and reproduction in any medium, provided the original work is properly cited.

Comparison of Flexible and Rigid Vegetation Induced Shear Layers in Partly Vegetated Channels

Gerardo Caroppi^{1,2} , Kaisa Västilä¹ , Paola Gualtieri² , Juha Järvelä¹ , Maurizio Giugni² , and Paweł M. Rowiński³ 

¹Department of Built Environment, Aalto University School of Engineering, Espoo, Finland, ²Department of Civil, Architectural and Environmental Engineering, University of Naples Federico II, Naples, Italy, ³Institute of Geophysics, Polish Academy of Sciences, Warsaw, Poland

Abstract Natural riparian vegetation generally presents a complex hydrodynamic behavior governed by plant morphology and flexibility. By contrast, hydrodynamic processes in partly vegetated channels are conventionally simulated by using simplified model vegetation, such as arrays of rigid cylinders. The aim of this study is to investigate the impacts of embedding natural plant features in the experimental simulation of flow in partly vegetated channels. Unique comparative experiments were carried out with both reconfiguring vegetation made of natural-like shrubs and grasses, and with rigid cylinders. While the lateral distributions of flow properties presented a high similarity governed by the shear layer differential velocity ratio, the bulk vegetative drag, and the presence of large-scale vortices, the flexibility-induced mechanisms of natural-like vegetation markedly affected the flow at the interface. Differences in plant morphology and spacing, and the dynamic motion of flexible foliated plants induced deeper vortex penetration into the vegetation. The normalized shear penetration was 6–10 times greater than observed for rigid cylinders, resulting in wider zones significantly exchanging momentum with the adjacent open water. The efficiency of lateral momentum transport for flexible foliated vegetation was up to 40% greater than the corresponding rigid cylinder case. Overall, the results indicated that improving the representativeness of model vegetation is a critical step toward the accurate simulation of hydrodynamic and transport processes in natural settings.

1. Introduction

In a variety of environmental settings, including vegetated channel banks and rivers, and their associated floodplains and riparian areas, vegetation occurs along river margins, partially obstructing the cross-section. In these systems, referred to as partly vegetated channels, the long regions of finite width of emergent vegetation laterally interact with the flow, deeply altering the mean and turbulent flow structure with implications on the conveyance capacity of the channel, the water levels, and the mass and momentum exchange processes (Aberle & Järvelä, 2013; Naot et al., 1996; Nepf, 2012; Rowiński et al., 2018).

Vegetation found along river margins and riparian areas is often composed of woody deciduous trees and shrubs (Schnitzler et al., 2007), with branches and leaves heterogeneously distributed over the height. Owing to its non-rigid hydrodynamic behavior and the high flexibility associated with plant subparts (Faisal et al., 2010; Gibson, 2012), natural vegetation exhibits bending and streamlining in response to the flow forcing. These processes, referred to as reconfiguration (Harder et al., 2004; Vogel, 1989), are associated with a reduction in drag (Boothroyd et al., 2017), particularly marked for foliated vegetation (Västilä & Järvelä, 2014; Whittaker et al., 2015; Wilson et al., 2008). Furthermore, the flow field modifications induced by the presence of vegetation are reflected in the dynamic response of vegetation itself (Ackerman & Okubo, 1993; Okamoto & Nezu, 2009). These two processes have been found to deeply influence the flow-vegetation interaction, affecting the exchange processes occurring at the interface between vegetation and the adjacent open water (Abdolahpour et al., 2018; Caroppi, Västilä, Järvelä, et al., 2019; Ghisalberti & Nepf, 2006) and are expected to markedly impact the flow structure in partly vegetated channels in presence of non-submerged foliated vegetation.

In partly vegetated channels, owing to the significantly different hydraulic resistance in the two regions of the channel, the flow in the lateral vegetated area is slower than that in the main channel. As a result, in analogy to canonical free shear layers, strong velocity gradients develop between the two areas of the

channel, making the flow susceptible to Kelvin-Helmholtz type instability (Brown & Roshko, 1974; Lesieur, 1995). Thus, the resulting horizontal vegetated shear layer can be effectively described using characteristic velocities defined for plane mixing layers, such as the low speed stream velocity (in the vegetated area) U_1 , the high speed stream velocity (in the main channel) U_2 , the convection velocity $U_c = (U_1 + U_2)/2$, the differential velocity $\Delta U = U_2 - U_1$, and the normalized velocity difference or differential velocity ratio $\lambda = \Delta U / 2U_c$ (Ho & Huerre, 1984; Pope, 2000). Analogously, the mixing layer width δ , defined as the cross-flow distance between positions where velocities attain the ambient flow values within 10% of accuracy, and the momentum thickness $\theta = \int_{-\infty}^{+\infty} \left\{ (1/4) - \left[(U(y) - U_c) / \Delta U \right]^2 \right\} dy$, can be used as representative characteristic lengths.

The presence of vegetation plays a key role in the shear layer dynamics by governing the overall drag faced by the flow in the lateral vegetated area and, consequently, by setting the total velocity difference. Indeed, in partly vegetated channels, the onset of large-scale (LS) turbulent coherent structures has been linked to the differential velocity ratio λ (Caroppi, Gualteri et al., 2020; Dupuis et al., 2017; Proust et al., 2017). LS vortices govern the exchange processes between the vegetated area and the main channel (Ghisalberti & Nepf, 2002; White & Nepf, 2007), playing a key role in riverine ecosystems by regulating the transport of sediments, nutrients and pollutant (Box et al., 2019; Jirka, 2001; Montakhab et al., 2012), with a variety of biological and ecological implications (e.g. Garcia et al., 2012; Pavlov et al., 2008; Walling et al., 2003).

Despite the non-rigid and dynamic flow-influencing hydrodynamic behavior of natural vegetation, hydrodynamic processes in partly vegetated channels have been conventionally investigated by simulating vegetation with morphologically simple elements, such as rigid cylinders (e.g. Dupuis et al., 2017; White & Nepf, 2008). Existing models of transverse exchange of momentum in lateral shear layers in partly vegetated channels (e.g. Truong & Uijtewaal, 2018; White & Nepf, 2008), velocity prediction models (e.g. Liu & Shan, 2019; Liu et al., 2020; Yan et al., 2020) and numerical simulations (e.g. Xiao et al., 2020; Xiaohui & Li, 2002; Xu et al., 2019) have been conceptualized, designed, calibrated and tested with reference to cylinders or rod-like rigid vegetation. The representativeness of rigid cylinders for simulating the presence of natural vegetation of complex morphology has not yet been explored (Caroppi, Västilä, Gualtieri, et al., 2019).

Recent studies have shown that using rigid, cylindrical elements for simulating natural vegetation can bias the study outcomes, by either hiding or amplifying some of the relevant physical processes found in natural conditions (Tinoco et al., 2020). For example, for vertical shear layers induced by submerged vegetation, significant differences in turbulent flow structure and momentum exchange have been observed for natural-like vegetation (dynamically scaled vegetation prototypes of aquatic seagrasses, blade-shaped tensile vegetation) relative to rigid cylinders, both for current- (Ghisalberti & Nepf, 2006; Termini, 2015) and wave-dominated flows (Abdolapour et al., 2018).

Flow-vegetation physical interactions and ecologically relevant mass-transfer processes depend on how characteristic physical scales match biological scales of vegetation (Nikora et al., 2012). The physical scales of hydrodynamic processes occurring in partly vegetated channels match the scales of plants and plant patch dimensions. Natural riparian vegetation typically presents a variable cross-sectional area over the water depth and, due to the presence of leaves, stems and branches, is characterized by multiple characteristic lengths (Albayrak et al., 2014; Västilä & Järvelä, 2018). In addition, the spacing between woody foliated plants, measured as the distance between plant stems at the bed, is larger than generally assumed for cylinder arrays, with this parameter being not representative of the spatial distribution of plant material. Such distribution is temporally and spatially variable and is a function of the flow velocity (Tinoco et al., 2020). Thus, riparian woody foliated vegetation cannot be reduced into arrays of simple cylindrical shaped elements and cannot be described uniquely by characteristic lengths such as the cylinder diameter or the cylinder spacing (Aberle & Järvelä, 2015). In addition, the hydrodynamic behavior of vegetation, governed by plant flexibility (Boothroyd et al., 2017; Ghisalberti & Nepf, 2006; Siniscalchi et al., 2012), cannot be reproduced by rigid cylinders.

The aim of this study is to investigate the hydrodynamic differences associated with two alternative vegetation representations in partly vegetated channels, highlighting benefits and disadvantages of using rigid cylinders and natural-like vegetation. Experiments carried out with complex morphology reconfiguring plants

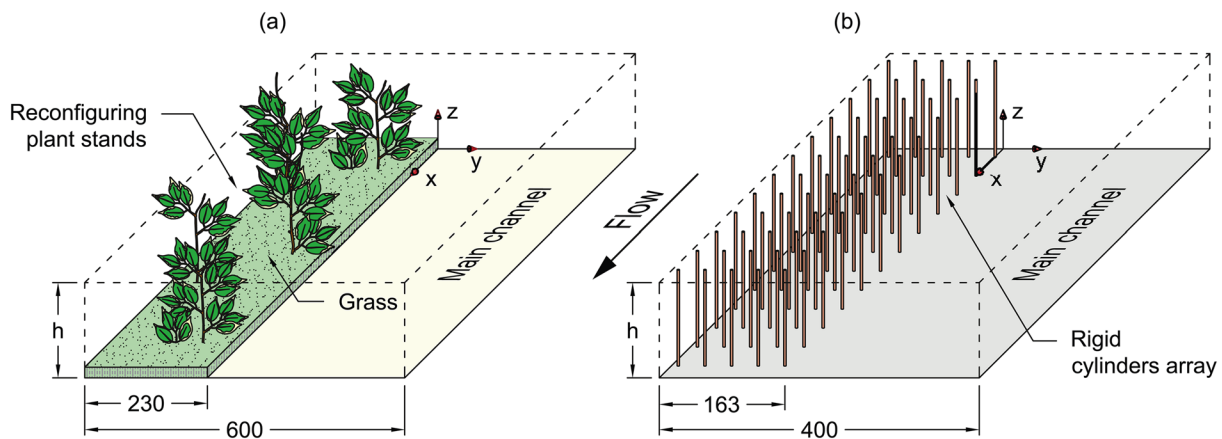


Figure 1. View of the experimental flumes with specification of vegetation elements and arrangement, channel width, vegetated area width, and flume coordinate system, for *F* (a) and *R* (b) experimental facility. All dimensions are in millimeters.

at the Environmental Hydraulics Lab of Aalto University and with rigid cylinders at the Laboratory of Hydraulics of University of Naples Federico II were used for establishing a novel comparative analysis, with a specific focus on hydrodynamic parameters governing key exchange processes at the vegetative interface.

2. Materials and Methods

Two sets of experiments were established for comparing the horizontal shear layers induced by natural-like vegetation and rigid cylinders in a partly vegetated channel. The first set, indicated as *F* experiments, was carried out at the Environmental Hydraulics Lab of Aalto University, in a flume partly covered by reconfiguring plants standing on a grassy understory (Section 2.1, Figure 1a). The second set, indicated as *R* experiments, was performed at the Laboratory of Hydraulics of University of Naples Federico II, where the presence of vegetation was simulated by using rigid cylinders (Section 2.2, Figure 1b).

For both the experimental setups, the x , y , and z axes of the coordinate system referred to the longitudinal, lateral, and vertical (normal to the flume bottom) directions, respectively. The coordinate system origin was defined as $x = 0$ at the inlet cross-section, positive downstream; $y = 0$ at the interface of the vegetated region (the edge of the grassy bed for *F* tests and the outer cylinders row for the *R* tests) and positive toward the main channel; and $z = 0$ at the top of the flume bed and positive upwards (Figure 1). In this right-handed Cartesian coordinate system, velocity components were denoted as u , v and w , in the x , y , and z directions, respectively.

For the two sets of tests, the flow velocity was investigated along transversal middepth transects using acoustic Doppler velocimetry (ADV). The agreement between the middepth measurements and the depth-averaged velocity was verified by measuring several vertical velocity profiles. For the *F* tests, an average deviation of 15% was observed for the verticals within the vegetation, with higher values observed at the outer part of the vegetated region. For rigid cylinders, for which the frontal projected area of vegetation was uniform over the height, nearly uniform velocity distributions were observed, in agreement with the observations of White and Nepf (2008) and Kubrak et al. (2008). The investigated transects were located in the fully developed region of the flow identified by acquiring velocity measurements along the flume at different longitudinal locations.

The raw ADV data were pre-filtered discarding values with signal-to-noise ratio and correlation lower than 15 dB and 70%, respectively, and despiked with the Velocity Signal Analyzer software (v1.5.64) (Jesson et al., 2015). Full research data associated to this study are available in a public repository (Caroppi et al., 2020a), and are described and completed by a data article (Caroppi et al., 2020b). The data used for the novel comparative analysis described in this study are part of two larger data sets collected in the framework of a broader research project on flow-vegetation interaction in partly vegetated channels (Caroppi, Gualteri et al., 2020; Caroppi, Västälä, Gualtieri, et al., 2019). Even constituting two independent data sets,

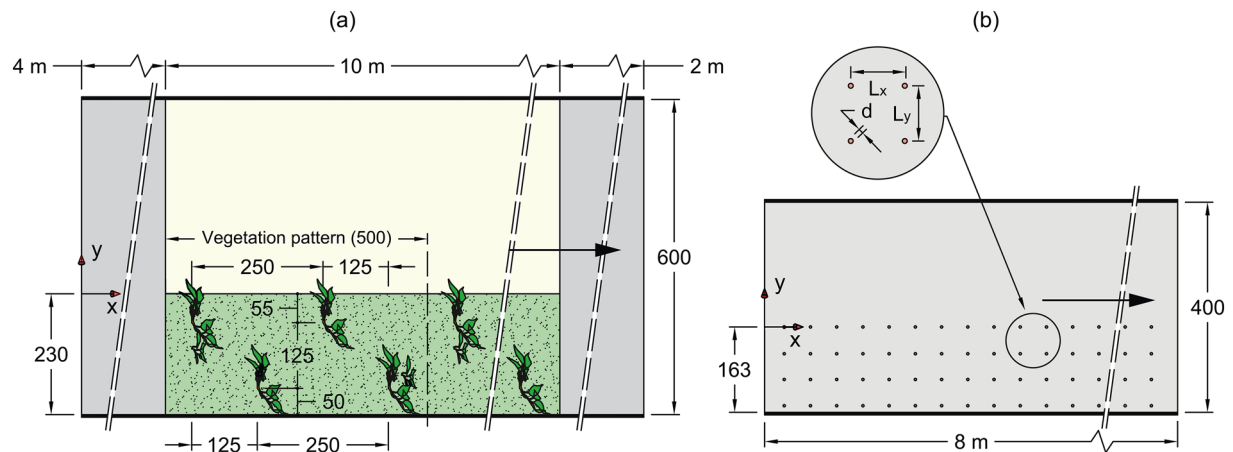


Figure 2. Top view of experimental flume for F (a) and R (b) tests, with indication of vegetation element spacing. All dimensions are in millimeters unless otherwise indicated.

the experiments with rigid cylinders were accurately designed to match, according to the criteria described in Section 2.3, the experiments with natural-like vegetation.

2.1. Experiments With Natural-Like Vegetation: F Cases

Experiments were carried out in a 20 m long, 0.6 m wide, and 0.8 m deep tilting glass-walled recirculating flume at the Environmental Hydraulics Lab of Aalto University (Figure 2a). The flume bottom from 4 to 14 m from the inlet was covered with a 600 mm wide PVC base plate, onto which the vegetation elements and the grass lining were installed. The slope of the flume and the position of a downstream tailgate were adjusted to achieve uniform flow conditions, with a 170 mm water depth for all the examined cases. Water depths were measured at multiple longitudinal locations with pressure sensors (accuracy ± 3 mm). Approximately 40% of the flume width was covered by an array of emergent artificial foliated plant stands. In order to increase the similarity with natural riparian conditions, where shrubby and woody vegetation stand on a grassy understory (Berends et al., 2020; Lecercf et al., 2016), a 20 mm tall and 230 mm wide artificial grass lining was selected as bed roughness in the vegetated area. The presence of bed grasses allowed to reproduce realistic near-bed flow whereas preliminary tests carried out in absence of bed grasses revealed that longitudinal velocity peaked in the near-bed region owing to the smooth bed and the reduced frontal projected area of the plants in the first 2–3 cm. The vegetation model was made of four different plants and two low leaf clusters to form a 0.5 m long repetitive pattern (Figure 2a). Each plant was composed of a vertical stem (with 3.8 mm average diameter) and 3–4 lateral foliated branches, each with four leaves (Figure S1). Each low leaf cluster was a single branch with four leaves connected to the bed (Figure S1). The plant stands were arranged in a staggered pattern with a longitudinal L_x and lateral L_y spacing of 250 and 125 mm, respectively. The number of plant stands per m^2 of vegetated bed area m was equal to 35. The bulk solid volume fraction ϕ of the vegetation was equal to 0.12%. Following Västilä et al. (2013), the ratio between the one-sided frontal leaf area and the stems frontal projected area, A_L/A_S , was used for describing such woody foliated vegetation. The vegetation bulk A_L/A_S , evaluated using image analysis (Text S1), was equal to 32 ± 1 , thus close to the median value of the data compiled by Västilä and Järvelä (2014) for common deciduous riparian species across a range of plant size from seedlings ($A_L/A_S = 30$ –70), to saplings ($A_L/A_S = 6$ –19) and mature trees ($A_L/A_S = 1$ –13). Drag force measurements on the isolated plants were used to assess the representativeness of the vegetation hydrodynamic behavior (Text S2 and Figure S2).

In order to take into account the effects of reconfiguration, the same vegetation was tested under three different cross-section-averaged bulk velocities U_m of 0.22, 0.49, and 0.82 m/s, resulting in three test cases $F1$, $F2$, and $F3$, with progressively increasing plants reconfiguration (Table 1, Text S3 and Figure S3). For the three investigated conditions, vegetation was emergent with negligible difference in submerged leaf area. Three dimensional velocity components were measured at 200 Hz with a Nortek Vectrino + ADV with a 4-beam side-looking probe (accuracy $\pm 1\%$). A recording time of 120 s (24,000 samples) was found to be

Table 1
Relevant Shear Layer Quantities for F and R Test Cases

Run	U_m (m/s)	h (mm)	U_1 (m/s)	U_2 (m/s)	ΔU (m/s)	U_C (m/s)	λ (-)	$C_D a$ (m ⁻¹)	δ (mm)	θ (mm)	δ/θ (-)
λ_1 —Slightly reconfigured vegetation (F1) versus dense array of rigid cylinders (R1)											
F1	0.22(0.01)	170(3)	0.04(0.01)	0.37(0.00)	0.32(0.01)	0.20(0.00)	0.79(0.03)	11.4(6.7)	201(9)	37(1)	5.4(0.4)
R1	0.45(0.02)	84(1)	0.09(0.00)	0.84(0.01)	0.75(0.01)	0.47(0.00)	0.80(0.01)	10.5(1.7)	121(3)	21(0)	5.6(0.3)
λ_2 —Moderately reconfigured vegetation (F2) versus sparse array of rigid cylinders (R2)											
F2	0.49(0.03)	170(3)	0.21(0.01)	0.78(0.00)	0.57(0.01)	0.50(0.01)	0.58(0.01)	1.5(0.2)	176(8)	36(1)	4.9(0.4)
R2	0.59(0.03)	135(1)	0.23(0.01)	0.98(0.01)	0.74(0.01)	0.60(0.01)	0.61(0.01)	1.7(0.3)	100(3)	21(0)	4.7(0.3)
λ_3 —Strongly reconfigured vegetation (F3) versus very sparse array of rigid cylinders (R3)											
F3	0.82(0.04)	170(3)	0.53(0.01)	1.27(0.00)	0.74(0.01)	0.90(0.01)	0.41(0.01)	0.5(0.0)	144(4)	33(0)	4.4(0.3)
R3	0.65(0.03)	122(1)	0.38(0.01)	0.92(0.01)	0.54(0.01)	0.65(0.01)	0.41(0.01)	0.6(0.1)	90(5)	21(0)	4.2(0.4)

Note. U_m is the cross-section-averaged velocity, h the water depth, U_1 and U_2 are the equilibrium velocity in the vegetated area and the main channel, respectively, ΔU is the differential velocity, U_C the convection velocity, λ the differential velocity ratio, $C_D a$ the bulk vegetative drag-density parameter, δ the shear layer width, θ the momentum thickness. Numbers in parentheses indicate the uncertainty resulting from uncertainty in the definition of U_1 and U_2 , and from water depth measurements (Text S5).

sufficiently large to achieve statistically time-independent averaged velocity and turbulence parameters. The lateral distributions of flow velocity statistics were obtained by temporally and spatially averaging the measurements acquired along two transversal middepth transects, as to take into account the flow spatial variability due to the vegetation heterogeneity in the longitudinal direction. Point velocity measurements were taken every 5–20 mm, with the densest spacing used in the high gradient region of the velocity profile, resulting in overall 45 point measurements per transect (see Caroppi et al., 2020b for detailed information). For all the F tests, plant motion was observed and video-recorded during the experiments. The videos, showing the plants reconfiguration and dynamic coherent motion, are available in Mendeley Data (Caroppi et al., 2020a). Experiments with grasses only, in the considered partly vegetated conditions, were also carried out (not described herein).

2.2. Experiments With Rigid Cylinders: R Cases

Experiments were carried out in an 8 m long, 0.4 m wide, and 0.4 m high acrylic-walled recirculating flume, with 0.48% slope, at the Laboratory of Hydraulics of University of Naples Federico II (Figure 2b). Backwater profiles were experimentally determined along the channel midline using a gauging needle (accuracy ± 1 mm). Occurrence of critical flow conditions at the channel outlet and the manifestation of a subcritical gradually varied flow profile were observed for all runs. All the velocity measurements were performed in the reach of the flume where uniform flow conditions were present, ~ 4.5 m upstream of the channel outlet. The measuring section was ~ 3.5 m downstream of the channel inlet, where the effects of inlet-induced disturbance were negligible and the flow was fully developed.

The vegetation was simulated by an array of aligned emergent wooden cylinders with diameter $d = 4.5$ mm covering $\sim 40\%$ of the flume width for the entire flume length (Figure 2b). The cylinders spacing was varied to achieve different vegetation density described by the frontal projected area per unit volume $a = md$, with m being the number of cylinders per unit bed area. Three representative test cases R1, R2, and R3 were selected from a larger data set (Caroppi, Gualteri et al., 2020), following the criteria described in Section 2.3. Specifically, three different cylinder densities representative of dense, sparse and very sparse vegetation, with a equal to 7.2, 3.6, and 0.9 m⁻¹, respectively, were considered (Table 1). L_x was equal to 25, 25, and 100 mm, while L_y was equal to 25, 50, and 50 mm for R1, R2, and R3, respectively. The position of the main channel-vegetation interface and the width of the vegetated region B_V were kept constant in all runs. The density reduction was achieved by progressively reducing the number of cylinders.

Three dimensional velocity components were measured at 100 Hz with a Nortek Vectrino II ADV with a 4-beam down-looking probe (accuracy $\pm 1\%$). A recording time of 240 s (24,000 samples) was used. The fully

developed flow was investigated by acquiring one transversal middepth transect, located at $L_x/2$ between two successive rows of cylinder within the measurement section. Point velocity measurements were taken every 5–10 mm, with the densest spacing used in the high gradient region of the velocity profile, resulting in overall 40 point measurements per transect (see Caroppi et al., 2020b for details). The flow longitudinal spatial variability within the cylinder array is beyond the scope of this research.

2.3. Vegetated Shear Layer Similarity

The different morphology and hydrodynamic behavior associated to the two vegetation representations make establishing a direct comparison between natural-like plants and rigid cylinders a challenging task. Therefore, rather than establishing a geometric comparison, in the light of the large-scale effects that the presence of vegetation induced on the flow, the similarity between the two configurations was established in terms of resulting vegetated shear layer hydrodynamic features and overall vegetative drag. Specifically, the similarity between the two sets of shear layers was achieved by matching two key parameters: the normalized velocity difference λ , and $\langle C_{Da} \rangle$, the overall bulk vegetative drag per unit water volume. λ provides information on the overall strength of the shear layer by measuring the relative magnitude of the total shear compared to the convection velocity (Ho & Huerre, 1984). $\langle C_{Da} \rangle$ depends on both the velocity within the vegetated region and the vegetation response to the flow forcing, accounting for vegetation morphology, density, and reconfiguration. $\langle C_{Da} \rangle$ was estimated assuming the equilibrium between the bulk vegetative drag and the pressure gradient and neglecting the contribution of the interface turbulence stress in driving the flow within the vegetation (Caroppi, Västilä, Järvelä, et al., 2019; White & Nepf, 2008) as:

$$0.5\langle C_{Da} \rangle U_1^2 = gi, \quad (1)$$

where U_1 is the equilibrium velocity within the vegetation, g is the gravitational acceleration, and i is the channel slope. In order to enhance the similarity between the two sets of experiments, the percentage of the cross-section occupied by vegetation B_v/B was kept equal to $\sim 40\%$ for both the experimental configurations, while keeping comparable the water depth to channel width ratio $h/B \approx 30\%$ among the test runs.

To allow the comparison between natural-like vegetation and rigid cylinders, the test cases with foliated plants exhibiting increasing reconfiguration (from $F1$ to $F3$) were respectively paired with test runs with progressively decreasing cylinders density (from $R1$ to $R3$) (Table 1). Specifically, the reconfiguration-induced vegetative drag reduction of natural-like vegetation was reproduced by reducing the cylinder density. This resulted in defining three pairings of similar shear layers, λ_1 , λ_2 , and λ_3 , each characterized by analogous λ and $\langle C_{Da} \rangle$: (λ_1) slightly reconfigured foliated vegetation versus dense array of rigid cylinders; (λ_2) moderately reconfigured foliated vegetation versus sparse array of rigid cylinders; (λ_3) strongly reconfigured foliated vegetation versus very sparse array of rigid cylinders. The details of the selected test cases and the shear layer characteristic parameters are reported in Table 1. The three pairings of test runs were characterized by decreasing velocity ratio λ , equal to 0.8, 0.6 and 0.4, respectively, and bulk vegetative drag-density parameter, approximately equal to 10.9, 1.6 and 0.6 m^{-1} , respectively. For all the runs the presence of LS coherent structures with characteristic Strouhal number approximately equal to 0.032 was observed in the shear dominated region of the flow (Figure S4 and Text S4). The shear layer characteristic Reynolds number $Re_\theta = \Delta U \theta / \nu$ (with ν being the water kinematic viscosity) and the main channel characteristic Reynolds number $Re_h = U_2 h / \nu$ ranged between 11,500–24,000 and 60,000–200,000, respectively, indicating that the shear layers were fully turbulent.

The differences existing in dimensional and geometrical features of the two experimental setups, such as the flume width (B), the vegetation representation (plants vs. cylinders), the vegetated region width (B_v), and the differences in dimensional characteristic velocities and lengths among the resulting shear layers (ΔU , θ , δ), do not hinder the comparability between the two sets of shear layers. Indeed, the similarity of such flows, enhanced by the presence of LS vortices (Raupach et al., 1996), has been demonstrated across a wide range of systems and length scales (Ghisalberti, 2009).

For each pairing of shear layers, it should be taken into account that the process inducing the drag and velocity ratio reduction from λ_1 to λ_3 was different among F and R cases. For the natural-like vegetation, owing to the increasing cross-section-averaged velocity (from $F1$ to $F3$), the vegetation experienced a progressively

increasing reconfiguration (Figure S3 and videos, Caroppi et al., 2020a), with $\langle C_D a \rangle$ reduced by a factor of ~ 20 . For rigid cylinders, the drag reduction was achieved by decreasing m from 1600 (R1) to 200 (R3) cylinders/m², thus presenting a reduction $>85\%$. Foliated reconfiguring plants exhibited coherent motion (videos, Caroppi et al., 2020a), in analogy with submerged flexible vegetation exhibiting “monami” (Ackerman & Okubo, 1993; Okamoto & Nezu, 2009). The dominant frequency of oscillation of the outermost plants matched the frequency corresponding to the peak in the velocity spectra (Caroppi, Västilä, Järvelä, et al., 2019). Due to the lateral motion of the plants, the lateral position of the interface, as evaluated in Caroppi, Västilä, Järvelä, et al. (2019) and defined by the average position of the outermost plant elements, varied among F1–F3.

In the following, the comparison between the test cases of Table 1 is conducted in terms of normalized lateral distributions of velocity statistics. For R cases, the flow properties were laterally averaged within the vegetated region using a moving average filter of window length L_y (Text S6 and Figures S5–S9). Flow features were normalized by adopting ΔU and θ as characteristic scaling velocity and length, respectively. The lateral coordinate was normalized as $(y-y_i)/\theta$, where y_i is the position of the inflection point in the lateral distribution of velocity. Differently from plane mixing layers, where the geometrical center of the layer and the position of the inflection point coincide, for vegetated shear layers this cannot be assumed a priori (Dupuis et al., 2017; Ghisalberti & Nepf, 2006). Considering that the inflection point is the primary source of flow instability (Fjørtoft, 1950), we assumed the inflection point position as a reference.

2.4. Turbulence Statistics and Drag Lateral Distribution

The description of the flow structure in the next section is based on temporally averaged velocity statistics. The mean flow field was described by the longitudinal average velocity U and the Reynolds stress τ_{xy} , as described by the lateral-longitudinal fluctuating velocities covariance $-cov_{uv}$. Lateral distributions of Reynolds stress were used for estimating the shear penetration w_p within the vegetation. w_p provided information on the extent of the exchange zone, i.e. the region within the vegetation actively exchanging momentum with the adjacent open water (Ghisalberti & Nepf, 2005; Murphy et al., 2007; Okamoto & Nezu, 2009). In analogy with shear penetration in submerged canopies (Caroppi et al., 2018; Nezu & Sanjou, 2008), w_p was evaluated as the distance between the vegetated interface and the lateral position where the Reynolds stress decayed to 10% of its maximum value.

The turbulent flow structure was described by the turbulent kinetic energy (TKE), providing information on the total turbulence intensity, and defined as $k = 0.5(\sigma_u^2 + \sigma_v^2 + \sigma_w^2)$, with σ_u^2 , σ_v^2 and σ_w^2 being the variance of the u , v and w , respectively. The turbulent correlation coefficient, i.e. the Pearson correlation coefficient between longitudinal and lateral turbulent fluctuations, $r_{uv} = cov_{uv}/(\sigma_u \sigma_v)$ was used for quantifying the efficiency of the turbulent lateral transport of streamwise momentum (Kaimal & Finnigan, 1994; Roth & Oke, 1995).

In partly vegetated channels with streamwise uniform flow, the momentum exchange between the main channel and the vegetated area can be analyzed referring to the time-averaged, spatially averaged, and depth averaged two-dimensional shallow water equations (Truong & Uijttewaai, 2018; White & Nepf, 2007). Indicating the depth averaging with the subscript d , the time and spatial horizontal averaging with an overbar and angled brackets, respectively, the simplified momentum exchange equation for a partly vegetated channel can be written as:

$$0 = -g \frac{dnh}{dx} + \frac{1}{\rho} \frac{dn\langle T_{xy} \rangle_d}{dy} - D, \quad (2)$$

where h is the water depth; n is the porosity of the vegetation canopy, $n = 1 - \phi$; ρ is the water mass density, and g the gravitational acceleration; $\langle T_{xy} \rangle_d$ is the total shear stress averaged over the water depth, in space and time, composed of viscous, Reynolds, dispersive and secondary circulation contributions; D is the drag force exerted on the fluid in the streamwise direction. Within the vegetated region $D = \langle 0.5 \rangle_d \bar{u}_d^2 C_D a$, in which $C_D a$ is the local value of the drag-density parameter, accounting for vegetation and bed drag, and $\langle \bar{u} \rangle_d$ is

the time-, space- and depth-averaged velocity. In the main channel $D = \langle 0.5 \rangle \bar{u}_d^2 c_f / h$, with c_f being the bed friction coefficient.

For shear layers characterized by high Reynolds numbers, the contribution of viscous stress can be neglected. Furthermore, for most conditions, the stress from secondary circulations is negligible (Prooijen et al., 2005; White & Nepf, 2008) and, in the range of the analyzed densities, the dispersive stresses are also relatively small compared to the Reynolds stress (Poggi, Katul et al., 2004; Poggi, Porporato et al., 2004; Truong & Uijttewaal, 2018). In this way, as generally observed for flow in vegetated regions at high Reynolds number, the Reynolds stress is the main shear stress (Truong & Uijttewaal, 2018) and $\overline{T_{xy,d}}$ can be approximated by $-\rho \langle u'v' \rangle_d$. Approximating the depth averaged quantities with the corresponding mid-depth measured values (Ben Meftah & Mossa, 2016; Truong & Uijttewaal, 2018; White & Nepf, 2007), and considering spatially averaged velocity and Reynolds stress within the vegetated area, Equation 2 can be rewritten as:

$$0 = ngi - n \frac{d(\text{cov}_{uv})}{dy} - D, \quad (3)$$

where D is equal to $0.5U^2 C_D a$ in the vegetated region, accounting for bed and plants drag, and $0.5U^2 c_f / h$ in the main channel. In uniform flow conditions, the quantity $-dh/dx$ in Equation 2, can be replaced by i , the channel slope. For the F tests, the solid volume fraction of the canopy was equal to 0.12%. For rigid cylinders, ϕ was equal to 2.54%, 1.27%, and 0.32% for R1, R2, and R3, respectively. Considering the low solid volume fraction, $n = 1$ was used in the calculation of D . In this study, Equation 3 was used to provide rough estimates of the local drag lateral distributions. For the flow within the vegetated region, with laterally constant velocity, Equation 3 simplifies into Equation 1, used for deducing the $\langle C_D a \rangle$ values of Table 1.

3. Results and Discussion

3.1. Mean Flow Structure and Shear Penetration

The normalized lateral distributions of mean velocity are shown in Figures 3a, 3b, and 3c. For each pairwise comparison, the distributions collapsed on the same curve within the shear layer, with greater differences within the vegetation with increasing plants reconfiguration. Indeed, even though the plant stands spatial arrangement was unvaried between the F cases, the increasing plant streamlining resulted in a progressively increasing flow spatial variability at the scale of the plants lateral spacing. For R tests, instead, the flow lateral spatial variability always matched the cylinder lateral distribution (Text S6 and Figures S5–S9). The similarity between the shear layers of each pairing was confirmed by the ratio δ/θ , a shear layer shape factor relating two length scales of the same velocity profile. δ/θ decreased with decreasing λ and was equal to ~ 5.5 , ~ 4.8 , and ~ 4.3 for λ_1 , λ_2 , and λ_3 , respectively (Table 1). The position of the inflection point (i.e. $(y-y_i)/\theta = 0$) relative to the position of the vegetated interface (dashed and solid black lines in Figure 3) varied depending on both the vegetation representation (between F and R cases at each λ) and the differential velocity ratio and overall bulk vegetation drag (from λ_1 to λ_3). For flexible vegetation, the inflection point was located within the vegetated area (F1 and F2 cases, Figures 3a and 3b), whereas, for rigid cylinders, the position of the inflection point and the interface were approximately coincident (R1 and R2 cases, Figures 3a and 3b). For λ_3 pairing (F3 and R3 test cases, Figure 3c) the inflection point was located on the main channel side of the interface.

Significant differences in shear penetration within the vegetation were observed, although the lateral distribution of normalized velocity presented a common trend mainly governed by λ and $\langle C_D a \rangle$. In Table 2, the shear penetration w_p normalized by θ are reported for each test case, as evaluated from the lateral distribution of Reynolds stress of Figures 3d, 3e, and 3f. From λ_1 to λ_3 , the shear penetration progressively decreased. w_p/θ was ~ 6 – 10 times higher within the natural-like vegetation compared to rigid cylinders. For slightly and moderately reconfigured vegetation (F1 and F2), more of the shear layer developed within the vegetation than for the corresponding rigid cylinder cases (R1 and R2), for which the shear mostly developed into the main channel.

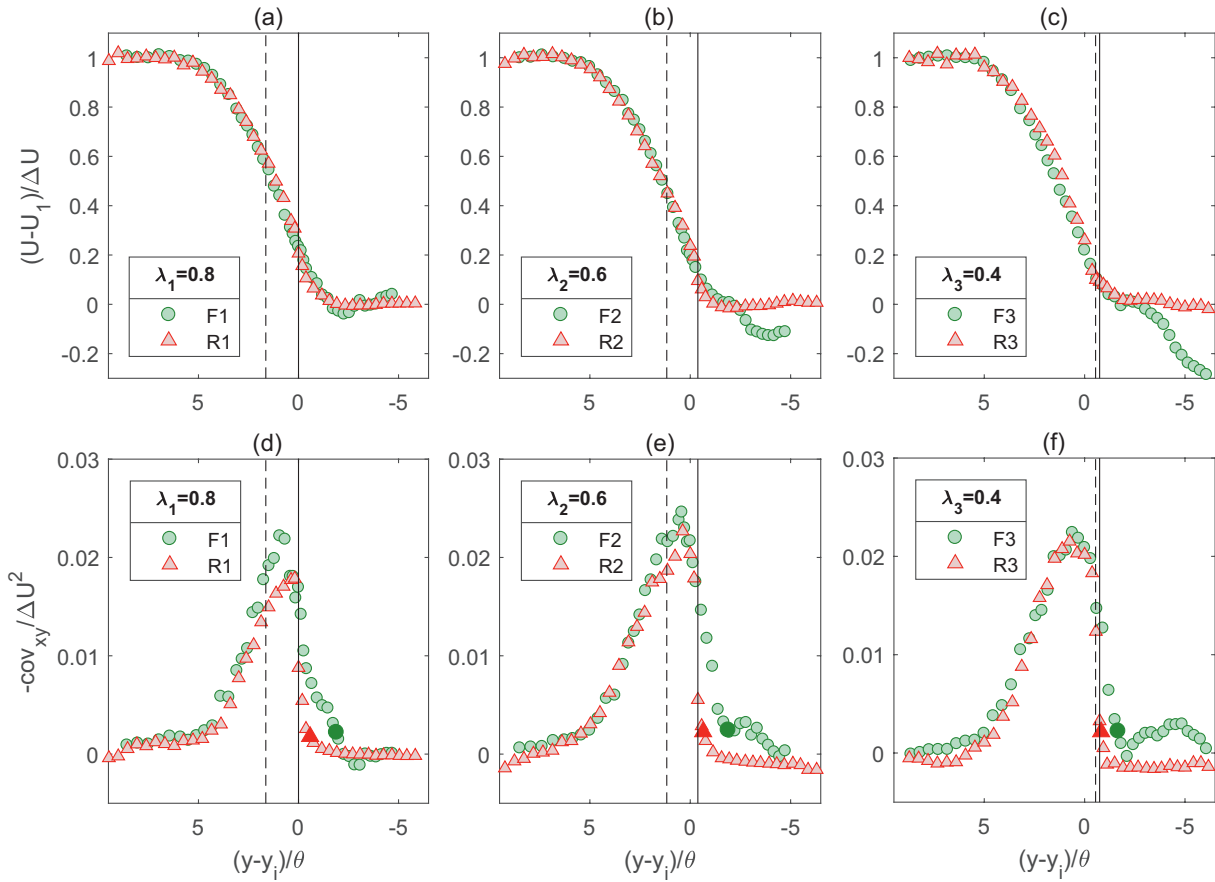


Figure 3. Lateral distributions of normalized longitudinal velocity for λ_1 (a), λ_2 (b), and λ_3 (c) pairing, and lateral distributions of normalized Reynolds stress for λ_1 (d), λ_2 (e), and λ_3 (f) pairing. The dashed line indicates the position of the vegetated interface for natural-like vegetation, whereas the solid line indicates the interface position for rigid cylinders. The point corresponding to the lateral position where the Reynolds stress decayed to 10% of its maximum value is indicated by a filled marker.

For dense vegetation, i.e. characterized by a non-dimensional flow-blockage factor $\langle C_D a \rangle B_v \geq 0.1$ (Belcher et al., 2003), the shear penetration has been found to scale with $\langle C_D a \rangle^{-1}$ (Poggi, Porporato, et al., 2004; Rominger & Nepf, 2011). Indeed, in previous studies with rigid cylinders, for shear layers induced by dense cylinder arrays and characterized by $\lambda \geq 0.8$, the penetration of the shear was found to increase with decreasing density (White & Nepf, 2008). In the current experiments, vegetation reconfiguration altered the obstruction flow-blockage factor, that varied from 2.6 of test case F1, consistent with dense canopies values, down to 0.1 of test case F3, thus consistent with characteristic values of sparse canopies (Table 2). Approximately the same variation was reproduced with rigid cylinders. For each comparison, the drag reduction

Table 2
Shear Penetration and Bulk Drag in the Main Channel and the Vegetated Region for F and R Test Cases

Pairing	$\lambda_1 = 0.8$		$\lambda_2 = 0.6$		$\lambda_3 = 0.4$	
Run	F1	R1	F2	R2	F3	R3
$C_D a$ (m ⁻¹)	11.4(6.7)	10.5(1.7)	1.5(0.2)	1.7(0.3)	0.5(0.0)	0.5(0.1)
$C_D a B_v$ (-)	2.6(1.5)	1.7(0.3)	0.3(0.1)	0.3(0.0)	0.1(0.0)	0.1(0.0)
w_p/θ (-)	3.5	0.6	3.1	0.3	1.1	0.1
$c_f/h/C_D a$ (-)	1%	1%	6%	3%	15%	16%
L_{x1}/δ (-)	1.2	0.1	1.4	0.3	1.7	1.1

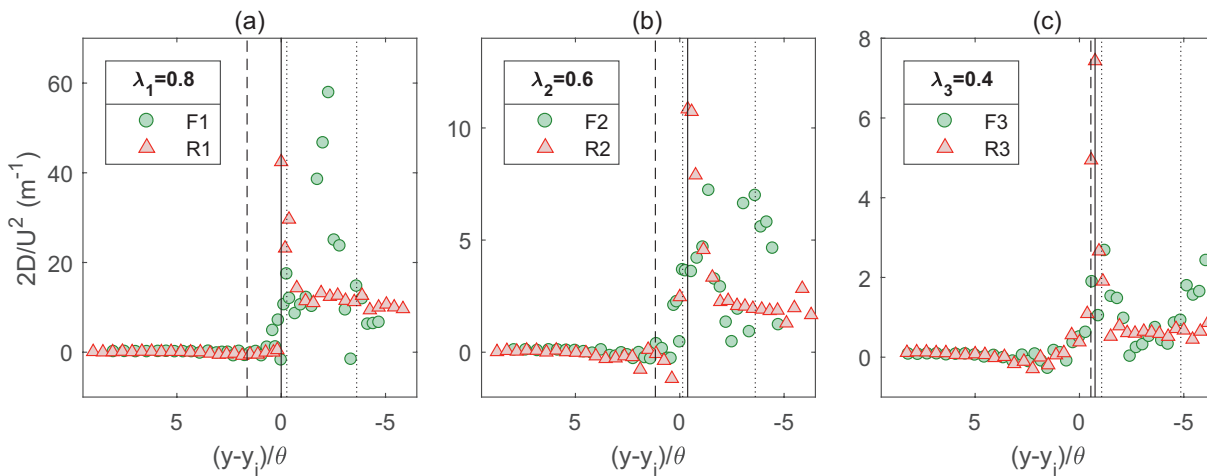


Figure 4. Lateral distributions of drag, as expressed by $2D/U^2$, for λ_1 (a), λ_2 (b), and λ_3 (c) pairing. The dashed line indicates the position of the vegetated interface for natural-like vegetation, whereas the solid line indicates the interface position for rigid cylinders. The lateral position of the two rows of plants (F experiments) are indicated by dotted lines.

was associated with a progressive reduction of differential velocity ratio, resulting in a different behavior in terms of shear penetration and overall shear layer features.

Owing to the drag difference between the vegetated area and the main channel, the normalized lateral distributions of Reynolds stress peaked at the interface, with the overall trend closely collapsing for F and R cases (Figures 3d, 3e, and 3f). For both R and F tests, the normalized Reynolds stress at the peak attained values higher than those observed for canonical plane mixing layers (Rogers & Moser, 1994), in agreement with the results of Marjoribanks et al. (2017) and Sukhodolov and Sukhodolova (2012) on vegetated shear layers induced by submerged vegetation. Differently from vertical shear layers induced by submerged vegetation, for which higher peaks have been observed for rigid vegetation relative to highly flexible blade-shaped vegetation (Ghisalberti & Nepf, 2006; Marjoribanks et al., 2017), the maximum normalized Reynolds stress attained comparable values among natural-like vegetation (0.023 ± 0.001) and rigid cylinders (0.021 ± 0.003). Difference in peak position and Reynolds stress lateral distributions were observed between F and R tests. For natural-like vegetation, the curve was slightly displaced toward vegetation, with the peak in Reynolds stress located on the vegetated side of the interface mean position. For cylinders, the Reynolds stress peaked directly on the main channel side of the interface. Going from λ_1 to λ_3 , with decreasing velocity ratio, the position of the peak in Reynolds stress progressively moved toward the main channel. Greater asymmetry of the distribution relative to the peak was observed for rigid cylinders, ascribable to the abrupt change in drag at the rigid vegetation interface, in contrast with the gradually changing drag in the dynamically moving outer part of the foliated vegetation.

3.2. Lateral Distribution of Vegetative Drag

For each pairing, the bulk drag exerted by the natural-like reconfiguring vegetative obstruction and by the rigid cylinders array, as described by $\langle C_D a \rangle$, assumed comparable values (Table 1), decreasing from $\sim 10.9 \text{ m}^{-1}$ of λ_1 down to $\sim 0.6 \text{ m}^{-1}$ of λ_3 . Nevertheless, differences in the local drag lateral distributions were observed. In Figure 4, the distributions of drag, as described by $2D/U^2$ and deduced from Equation 3, are reported. $2D/U^2$ is equal to the bed friction c_f/h in the main channel and to $C_D a$ in the vegetated region, with the latter accounting for the drag exerted by both vegetation and bed.

For natural-like vegetation, the lateral spatial variability in the drag-density parameter decreased with decreasing shear layer strength and bulk mean drag. From $F1$ to $F3$, the increasing plants streamlining progressively reduced the effects of plants morphological complexity on the flow. For slightly reconfigured vegetation, consistently with the observed shear penetration, $C_D a$ started increasing within the vegetated region with the greatest values observed between the two rows of plant stands ($F1$, Figure 4a). With increasing

reconfiguration, the local effect on drag induced by reconfigured plants increased, with peaks approximately located at plants lateral positions ($F2$ and $F3$, Figures 4b and 4c).

For rigid cylinders, the lateral distribution was unaffected by the overall shear layer velocity difference and, for all the test cases, the drag abruptly peaked at the interface, achieving, on average, an approximately constant value within the array. Nevertheless, all the R cases presented a high variability at the scale of the cylinder lateral spacing, as testified by the lateral distributions reported in the Figure S7. For all the test cases, the region of high $C_D a$ was located within the vegetation consistently with the observed shear penetration (Table 2) and the Reynolds stress distributions of Figures 3d, 3e, and 3f. The drag exerted by the bed into the main channel, as described by $\langle c_f/h \rangle$, the average c_f/h value in the constant velocity region within the main channel, assumed a progressively increasing relative importance on the overall shear layer dynamics, with the ratio $\langle c_f/h \rangle / \langle C_D a \rangle$ increasing from λ_1 to λ_3 (Table 2).

For F tests, the vegetation model was composed of foliated plants standing on a grassy bed. The plants exhibited strong reconfiguration whereas the grasses presented negligible reconfiguration, remaining fairly erect during the tests (Figure S3). Thus, when considering the decrease in $\langle C_D a \rangle$ observed from $F1$ to $F3$, it should be taken into account that the relative effect of grasses on the total drag progressively increased. Therefore, the variation in $\langle C_D a \rangle$ due to reconfiguration of the plants without grasses can be even higher than observed in our experiments.

3.3. Turbulent Kinetic Energy and Efficiency of Momentum Exchange at the Interface

The lateral distributions of normalized total TKE shown in Figures 5a, 5b, and 5c allow exploring the effects of vegetation representation on the turbulent flow structure. For all the investigated flows, the shear at the interface between the vegetated region and the main channel was the main source of TKE and, thus, all the profiles presented a peak approximately located at the interface.

For $F1$ and $F2$ cases, k peaked on the vegetated side of the interface and gradually decayed moving deeper into the vegetated region, with a roughly symmetrical distribution. For rigid cylinders, instead, k peaked at the interface and suddenly decayed within the vegetation, showing a gradual decay into the main channel. Consistently with the differences in shear penetration for natural-like vegetation and rigid cylinders (Table 2), the shear-related turbulence penetrated deeper into the vegetated region for natural-like vegetation, with a decreasing trend with decreasing λ . With decreasing $\langle C_D a \rangle$ and λ , from λ_1 to λ_3 , the similitude between the F and R case increased. The lateral distribution of TKE within the main channel, far from the interfacial exchange zone, was unaffected by the vegetation representation.

The three fluctuating velocity components contributed differently to the total TKE depending on the vegetation representation. For natural-like vegetation, on average 50% of k was produced by u' , with v' and w' contributing 20% and 30%, respectively. For rigid cylinders, the TKE was equally produced by u' and v' , with negligible contribution of w' ($\sim 5\%$), which agreed with the equal contribution of u' and v' reported by Tanino and Nepf (2007). Thus, relative to rigid cylinders, lower turbulence intensity of v' was observed for natural-like vegetation. This difference can be ascribed to the different morphology and hydrodynamic behavior of natural vegetation. When facing emergent vertical rigid cylinders, the flow is forced to deviate mainly in the lateral direction. On the contrary, in the presence of flexible vegetation of complex morphology, presenting submerged subparts with different orientation, the flow can deviate in both the vertical and lateral directions. Furthermore, owing to the vegetation streamlining and dynamic motion induced by the mean and turbulent flow field, the flow can keep moving forward, bending the plant element, and partly deviating in the transversal directions. As a consequence, for F tests, despite the lower absolute amount of turbulence related to v' , the turbulence associated with LS coherent structures (observed at the interface for all the considered test cases, Text S4 and Figure S4) was more efficient in laterally transferring momentum, as demonstrated by the lateral distributions of the turbulent correlation coefficient r_{uv} (Figures 5d, 5e, and 5f). Even though high efficiency of lateral momentum exchange was observed at the interface for both F and R tests owing to LS vortices, consistently higher values of $|r_{uv}|$ were observed for natural-like vegetation. Specifically, at the interface, $|r_{uv}|$ was equal to ~ 0.6 for natural-like vegetation, ~ 0.4 for rigid cylinders. Characteristic values of $|r_{uv}|$ for canonical mixing layers are equal to ~ 0.44 (Raupach et al., 1996), comparable to those observed in this study for rigid vegetation.

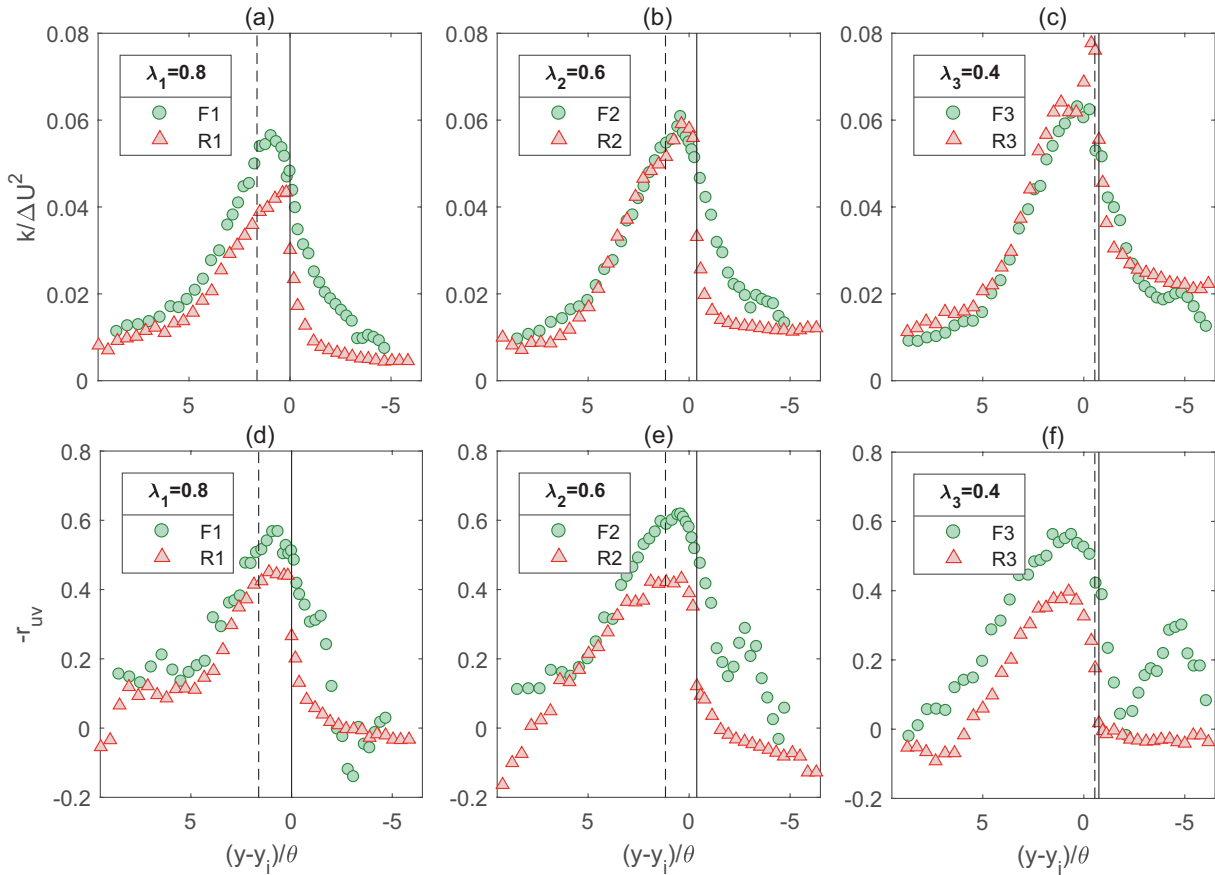


Figure 5. Lateral distributions of normalized TKE for λ_1 (a), λ_2 (b), and λ_3 (c) pairing, and lateral distributions of turbulent correlation coefficient for λ_1 (d), λ_2 (e), and λ_3 (f) pairing. The dashed line indicates the position of the vegetated interface for natural-like vegetation, whereas the solid line indicates the interface position for rigid cylinders. TKE, turbulent kinetic energy.

For $F1$ and $F2$ cases (Figures 5d and 5e), $|r_{uv}|$ peaked within the vegetation and progressively decayed deeper into the vegetated region. For rigid cylinders, instead, $|r_{uv}|$ peaked immediately at the main channel side of the interface and quickly dropped to lower values within the array. As a result, the exchange of momentum for natural-like vegetation took place over a larger portion of the vegetated region, in agreement with the observed w_p . High $|r_{uv}|$ indicates that a strong correlation exists between the two fluctuating velocity components. Specifically, values higher than 0.32 (the maximum boundary layer value) have been associated to LS coherent structures (Kaimal & Finnigan, 1994; Raupach et al., 1996). The lateral distributions of r_{uv} of Figure 5 indicate that differently from rigid cylinders, for foliated dynamically reconfiguring vegetation, LS coherent structures penetrated deeper into the vegetated region. This key observation provides the physical explanation to the differences observed at the interface between rigid and flexible vegetation.

3.4. Effects of Vegetation Morphology and Hydrodynamic Behavior

For each comparison, the similarity of $\langle C_D a \rangle$ and λ , and the presence of LS vortices resulted in pairwise similar flow structures. For each pairing, the flow velocity and the derived quantities all shared analogous normalized lateral distributions, presenting similar trend. The overall shape of the lateral distributions of flow properties were observed to change with decreasing $\langle C_D a \rangle$ and λ , with the inflection point of the velocity profile progressively shifting toward the main channel. Thus indicating that obstructed shear layers all share global features mainly governed by the magnitude of $\langle C_D a \rangle$ and λ , and the presence of LS vortices, independently from the features of the obstruction inducing the velocity difference. This conclusion is consistent with the observations of Ghisalberti (2009), who demonstrated the similarity of shear layers induced

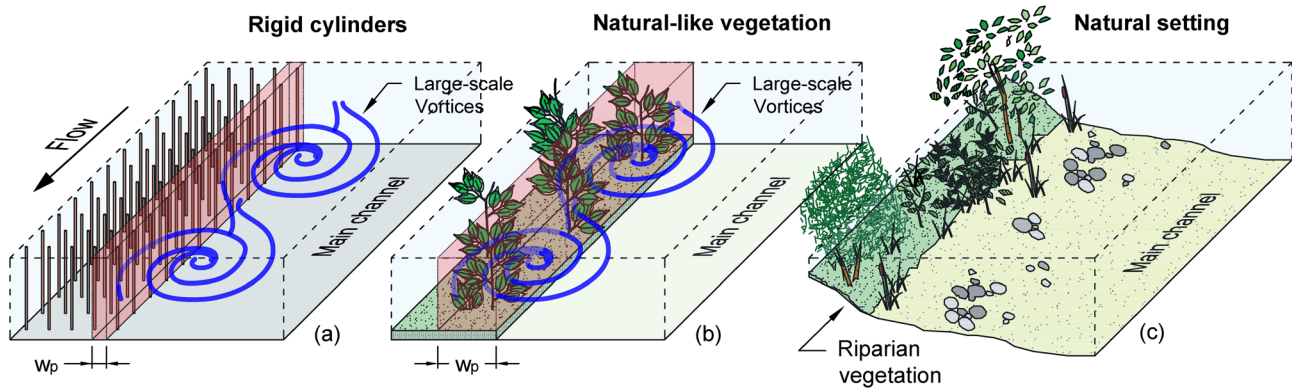
by submerged dense obstructions, including packed granular beds, vegetation canopies, coral reefs, and urban canopies. Our results, obtained on horizontal shear layers, confirm and extend the obstructed flow similarity to a wider range of systems and flow-blockage factors.

The similarity among F and R shear layers allowed isolating the main differences linked to the specific vegetation representation and associated with vegetation morphology, flexibility, and spatial arrangement. The morphological differences between foliated plants and cylinders led to inevitable different spatial distribution of individual elements constituting the canopy, with differences in spacing between elements at the interface (Figure 2). In addition, differently from rigid cylinders, the flexible nature and the morphological complexity of the foliated plants conferred a peculiar hydrodynamic behavior on the vegetation used in the F tests, exhibiting reconfiguration and dynamic motion. These two processes, following the concept of static and dynamic reconfiguration by Siniscalchi and Nikora (2013), can be viewed as the effects of the mean and the turbulent flow field, respectively. In response to the mean flow forcing, the flexible plants adapted their shape, with a progressive reduction of the average drag exerted on the flow (Figure S3). Moreover, in response to the turbulent flow field, natural-like vegetation exhibited pronounced dynamic motion, in analogy with submerged flexible vegetation exhibiting “*monami*” (Ackerman & Okubo, 1993; Okamoto & Nezu, 2009). This, was particularly evident at the interface, where the plants exhibited periodic motion, with marked lateral oscillations, in response to the periodic advection of LS coherent structures (Caroppi et al., 2020a, 2020b). These aspects, as described in the following, governed the vegetated shear layer dynamics, as emerged from the comparison with rigid cylinders.

The same vegetation arrangement exhibited a substantial drag variation induced by static reconfiguration (Figure S3), with $\langle C_D a \rangle$ going from 11.4 m^{-1} of slightly reconfigured vegetation ($F1$) down to 0.5 m^{-1} of strongly reconfigured vegetation ($F3$). To reproduce the effects of reconfiguration with rigid cylinders, the density of the array, as expressed by the frontal area per canopy volume, was modified from 7.2 ($R1$) to 0.9 m^{-1} ($R3$), respectively. The comparable bulk vegetative drag induced analogous velocity difference, with shear layers all characterized by the presence of LS coherent structures. Nevertheless, relevant differences in shear penetration, ascribable to the differences in morphology, spacing, and flexibility between foliated vegetation and cylinders were observed.

Assuming δ as a characteristic length of the LS vortices and being $L \approx L_x$ the average spacing between consecutive elements at the interface, the ratio L/δ can provide a measure of the canopy voids at the interface as compared to the size of the LS vortices. This ratio, in analogy with the argument used by Monti et al. (2020), can be used to partly explain the differences in vortex penetration. For the pairings with the strongest shear (λ_1 and λ_2), L/δ was ≥ 1 for foliated plants while, for rigid cylinders, was $\ll 1$ (Table 2), i.e. the spacing between cylinders set a limit for vortex penetration within the array. This observation can also justify the limited differences in shear penetration observed in this study between shear layers induced by dense arrays of aligned and staggered cylinders (Text S7, Tables S1 and S2, and Figure S10). Plants lateral periodic motion further enhanced the LS vortices penetration within the foliated flexible vegetation. By contrast, for rigid cylinders, as testified by the sudden drop in r_{uv} at the interface (Figures 5d, 5e, and 5f), the structure of the LS vortices was more effectively broken up by the non-waving rigid interface, diminishing its penetration within the vegetated region, in agreement with the analysis of Ghisalberti and Nepf (2002) for submerged vegetation. With decreasing $\langle C_D a \rangle$ and λ , the weaker shear layers progressively shifted toward the main channel leading to reduced penetration both for F and R tests (λ_3). As a consequence, the resulting exchange zone was notably wider for natural-like vegetation, with the lateral exchange of momentum taking place at the interface and driven by LS vortices being more efficient in comparison with rigid cylinders, as demonstrated by the higher value of r_{uv} . For F tests, the Reynolds stress penetrated into the vegetated region up to $\sim 65\%$ of the shear layer width, presenting a decreasing trend with decreasing $\langle C_D a \rangle$ and λ . For rigid cylinders, the shear penetration was limited at $\sim 10\%$ of δ , with analogous decreasing trend from λ_1 to λ_3 (Table 2).

Vegetation hydrodynamic behavior deeply affected the overall shear layer structure. Increasing vegetation reconfiguration (from $F1$ to $F3$) progressively reduced the effects of vegetation morphological complexity on the flow. With increasing plants streamlining, side twigs, leaves and stems were progressively less exposed to the flow. As a result, the similarity with rigid cylinders progressively increased going from λ_1 to λ_3 , with both types of vegetation representation inducing progressively greater local effects on the flow. For F tests, the flow spatial variability was limited and, owing to the variability of lateral distribution of plant material



Consideration for natural-like vegetation representation in simulations

- Tradeoffs are necessary to translate setting (c) to (b) but the use of natural-like vegetation properly reproducing vegetation morphology, spatial arrangement, and hydrodynamic behavior is superior to (a).
- The use of natural-like vegetation improves description of shear penetration w_p and momentum exchange processes associated with large-scale vortices.
- Proper description of plants' flexibility and foliage are key criteria affecting the mean and turbulent flow structure.

Figure 6. Synthesis of key implications of using natural-like vegetation in the simulation of vegetated flows. Schematization of flow in partly vegetated channel with rigid cylinders (a) and natural-like vegetation (b), example of typical natural setting (c).

with reconfiguration, increased with increasing bulk velocity. For R tests, the flow within the vegetated region patterned the cylinder lateral distribution, and local regions of high shear stress, drag and turbulence intensity (Figures S6–S8) developed within the array. These flow features, usually associated with staggered and aligned cylinders arrangement (Tinoco et al., 2020 and reference therein), locally alter the mass and energy transport processes within the vegetated region.

4. Concluding Remarks

The need to investigate hydrodynamic processes in natural systems (Figure 6c) has led to significant simplifications in representing vegetation in laboratory experiments and numerical simulations (Figure 6a). Even though such simplified settings have provided a detailed hydromechanical characterization of obstructed shear layers, their representativeness of natural conditions is still unexplored. In this study, a novel experimental setting closely representing conditions found along river margins was investigated (Figure 6). The results gained on the shear layer flows induced by natural-like vegetation were used to establish a unique comparative analysis with dynamically similar flows induced by rigid cylinders.

The use of rigid cylinders resulted in improper description of vegetated shear layers induced by foliated reconfiguring vegetation. The simplified vegetation representation allowed reproducing the main flow features universally characterizing obstructed shear layer flows presenting LS vortices. Nevertheless, even carefully matching bulk properties between F and R shear layers (Figures 6a and 6b), with all flows presenting LS coherent vortices, differences in vegetation morphology, spatial arrangement and flexibility induced systematic differences. For foliated reconfiguring vegetation, the normalized shear penetration w_p/θ , associated with the penetration of LS vortices within the vegetation, was 6–10 times greater than observed for rigid cylinders (Figures 6a and 6b). In addition, the efficiency of lateral momentum transport for natural like vegetation, as described by r_{lv} , was up to 40% greater than the corresponding rigid cylinder case. Thus, in comparison to rigid cylinders, the exchange processes occurring in natural riparian systems are expected to engage larger portions of the vegetated area and to be more efficient in transferring momentum across the interface and within the vegetated region. By analogy, similar differences are expected to affect the processes involving the transport of sediments, nutrients and pollutants.

Our comparison demonstrated that bulk flow properties such as $\langle C_{D\alpha} \rangle$ and λ are not enough to describe adequately the shear layer dynamics in presence of foliated reconfiguring vegetation. The use of rigid cylinders for simulating natural-like vegetation was not suitable to catch distinctive hydrodynamic features of vegetated shear layers. Incorporating natural plant properties in the experimental investigation resulted in

an improved description of shear penetration and momentum exchange processes associated to large-scale vortices. In conclusion, we argue that major improvements in the simulation of flow processes in natural vegetated settings are possible only when truly acknowledging the morphological and biomechanical properties of vegetation. Thus, adopting natural-like vegetation representation in the simulation of vegetated flows can play a fundamental role in advancing accurate description of hydrodynamic processes occurring in natural settings.

Conflict of Interest

The authors declare no conflicts of interest.

Data Availability Statement

Data for this research are available at Mendeley Data (Caroppi et al., 2020a) and are described by a data article (Caroppi et al., 2020b).

Acknowledgments

The authors thank the technician Antti Louhio for his help in arranging the experiments at the Environmental Hydraulics Lab of Aalto University. The authors acknowledge the support from the technicians Antonio Fusco and Domenico Palmiero of the Laboratory of Hydraulics of University of Naples Federico II. The authors acknowledge funding from Maa- ja vesiteknikan tukiry (Grant No. 33271), Maj and Tor Nessling Foundation (Grant No. 201800045), Academy of Finland (Grant No. 330217), and from statutory activities No. 3841/E-41/S/2020 of the Ministry of Science and Higher Education of Poland.

References

- Abdollahpour, M., Ghisalberti, M., McMahon, K., & Lavery, P. S. (2018). The impact of flexibility on flow, turbulence, and vertical mixing in coastal canopies. *Limnology & Oceanography*, 63(6), 2777–2792. <https://doi.org/10.1002/lno.11008>
- Aberle, J., & Järvelä, J. (2013). Flow resistance of emergent rigid and flexible floodplain vegetation. *Journal of Hydraulic Research*, 51, 33–45. <https://doi.org/10.1080/00221686.2012.754795>
- Aberle, J., & Järvelä, J. (2015). *Hydrodynamics of vegetated channels*. In Rivers-physical, fluvial and environmental processes (pp. 255–277). Springer. <https://doi.org/10.1007/978-3-319-17719-9>
- Ackerman, J. D., & Okubo, A. (1993). Reduced mixing in a marine macrophyte canopy. *Functional Ecology*, 7, 305–309. <https://doi.org/10.2307/2390209>
- Albayrak, I., Nikora, V. I., Miler, O., & O'Hare, M. T. (2014). Flow-plant interactions at leaf, stem and shoot scales: Drag, turbulence, and biomechanics. *Aquatic Sciences*, 76, 269–294. <https://doi.org/10.1007/s00027-013-0335-2>
- Belcher, S. E., Jerram, N., & Hunt, J. C. R. (2003). Adjustment of a turbulent boundary layer to a canopy of roughness elements. *Journal of Fluid Mechanics*, 488, 369–398. <https://doi.org/10.1017/S0022112003005019>
- Ben Meftah, M., & Mossa, M. (2016). Partially obstructed channel: Contraction ratio effect on the flow hydrodynamic structure and prediction of the transversal mean velocity profile. *Journal of Hydrology*, 542, 87–100. <https://doi.org/10.1016/j.jhydrol.2016.08.057>
- Berends, K. D., Ji, U., Penning, W. E., Warmink, J. J., Kang, J., & Hulscher, S. J. M. H. (2020). Stream-scale flow experiment reveals large influence of understory growth on vegetation roughness. *Advances in Water Resources*, 143, 103675. <https://doi.org/10.1016/j.advwatres.2020.103675>
- Boothroyd, R. J., Hardy, R. J., Warburton, J., & Marjoribanks, T. I. (2017). Modeling complex flow structures and drag around a submerged plant of varied posture. *Water Resources Research*, 53, 2877–2901. <https://doi.org/10.1002/2015WR017200.A>
- Box, W., Västilä, K., & Järvelä, J. (2019). The interplay between flow field, suspended sediment concentration, and net deposition in a channel with flexible bank vegetation. *Water*, 11, 24. <https://doi.org/10.3390/w11112250>
- Brown, G. L., & Roshko, A. (1974). On density effects and large structure in turbulent mixing layers. *Journal of Fluid Mechanics*, 64, 775–816. <https://doi.org/10.1017/S002211207400190X>
- Caroppi, G., Gualtieri, P., Fontana, N., & Giugni, M. (2018). Vegetated channel flows: Turbulence anisotropy at flow-rigid canopy interface. *Geoscience Series*, 8, 259. <https://doi.org/10.3390/geosciences8070259>
- Caroppi, G., Gualtieri, P., Fontana, N., & Giugni, M. (2020). Effects of vegetation density on shear layer in partly vegetated channels. *Journal of Hydro-Environment Research*, 30, 82–90. <https://doi.org/10.1016/j.jher.2020.01.008>
- Caroppi, G., Västilä, K., Gualtieri, P., Järvelä, J., Giugni, M., & Rowiński, P. (2019). Comparative analysis of lateral shear layers induced by flexible and rigid vegetation in a partly vegetated channel. In L. Calvo (Ed.), *Proceedings of the 38th IAHR World Congress (Proceedings of the IAHR World Congress)*. IAHR. <https://doi.org/10.3850/38WC092019-1310>
- Caroppi, G., Västilä, K., Gualtieri, P., Järvelä, J., Giugni, M., & Rowiński, P. M. (2020a). *Acoustic Doppler Velocimetry (ADV) data on flow-vegetation interaction in partly vegetated channels with flexible and rigid vegetation*. Mendeley Data. Retrieved from <https://doi.org/10.17632/p6m666p4kb.1>
- Caroppi, G., Västilä, K., Gualtieri, P., Järvelä, J., Giugni, M., & Rowiński, P. M. (2020b). *Acoustic Doppler velocimetry (ADV) data on flow-vegetation interaction with natural-like and rigid model plants in hydraulic flumes*. Data in Brief. <https://doi.org/10.1016/j.dib.2020.106080>
- Caroppi, G., Västilä, K., Järvelä, J., Rowiński, P. M., & Giugni, M. (2019). Turbulence at water-vegetation interface in open channel flow: Experiments with natural-like plants. *Advances in Water Resources*, 127, 180–191. <https://doi.org/10.1016/j.advwatres.2019.03.013>
- Dupuis, V., Proust, S., Berni, C., & Paquier, A. (2017). Mixing layer development in compound channel flows with submerged and emergent rigid vegetation over the floodplains. *Experiments in Fluids*, 58, 30. <https://doi.org/10.1007/s00348-017-2319-9>
- Faisal, T. R., Khalil Abad, E. M., Hristozov, N., & Pasini, D. (2010). The impact of tissue morphology, cross-section and turgor pressure on the mechanical properties of the leaf petiole in plants. *Journal of Bionic Engineering*, 7, 11–23. [https://doi.org/10.1016/S1672-6529\(09\)60212-2](https://doi.org/10.1016/S1672-6529(09)60212-2)
- Fjortoft, R. (1950). *Application of integral theorems in deriving criteria of stability for laminar flows and for the baroclinic circular vortex*. Geofys. Publication.
- García, X. F., Schnauder, I., & Pusch, M. T. (2012). Complex hydromorphology of meanders can support benthic invertebrate diversity in rivers. *Hydrobiologia*, 685, 49–68. <https://doi.org/10.1007/s10750-011-0905-z>
- Ghisalberti, M. (2009). Obstructed shear flows: Similarities across systems and scales. *Journal of Fluid Mechanics*, 641, 51–61. <https://doi.org/10.1017/S0022112009992175>

- Ghisalberti, M., & Nepf, H. M. (2002). Mixing layers and coherent structures in vegetated aquatic flows. *Journal of Geophysical Research*, 107, 1–11. <https://doi.org/10.1029/2001JC000871>
- Ghisalberti, M., & Nepf, H. M. (2005). Mass transport in vegetated shear flows. *Environmental Fluid Mechanics*, 5, 527–551. <https://doi.org/10.1007/s10652-005-0419-1>
- Ghisalberti, M., & Nepf, H. M. (2006). The structure of the shear layer in flows over rigid and flexible canopies. *Environmental Fluid Mechanics*, 6, 277–301. <https://doi.org/10.1007/s10652-006-0002-4>
- Gibson, L. J. (2012). The hierarchical structure and mechanics of plant materials. *Journal of The Royal Society Interface*, 9, 2749–2766. <https://doi.org/10.1098/rsif.2012.0341>
- Harder, D. L., Speck, O., Hurd, C. L., & Speck, T. (2004). Reconfiguration as a prerequisite for survival in highly unstable flow-dominated habitats. *Journal of Plant Growth Regulation*, 23, 98–107.
- Ho, C., & Huerre, P. (1984). Perturbed free shear layers. *Annual Review of Fluid Mechanics*, 16, 365–422. <https://doi.org/10.1146/annurev.fl.16.010184.002053>
- Jesson, M. A., Bridgeman, J., & Sterling, M. (2015). Novel software developments for the automated post-processing of high volumes of velocity time-series. *Advances in Engineering Software*, 89, 36–42. <https://doi.org/10.1016/j.advengsoft.2015.06.007>
- Jirka, G. H. (2001). Large scale flow structures and mixing processes in shallow flows. *Journal of Hydraulic Research*, 39, 567–573. <https://doi.org/10.1080/00221686.2001.9628285>
- Kaimal, J. C., & Finnigan, J. J. (1994). *Atmospheric boundary layer flows*. Atmospheric Research. Oxford University Press. [https://doi.org/10.1016/0169-8095\(95\)00045-3](https://doi.org/10.1016/0169-8095(95)00045-3)
- Kubrak, E., Kubrak, J., & Rowiński, P. M. (2008). Vertical velocity distributions through and above submerged, flexible vegetation. *Hydrological sciences journal*, 53, 905–920. <https://doi.org/10.1623/hysj.53.4.905>
- Lecerf, A., Evangelista, C., Cucherousset, J., & Boiché, A. (2016). Riparian overstorey-understorey interactions and their potential implications for forest-stream linkages. *Forest ecology and management*, 367, 112–119. <https://doi.org/10.1016/j.foreco.2016.02.031>
- Lesieur, M. R. (1995). Mixing layer vortices. In S. I. Green (Ed.), *Fluid vortices* (pp. 35–63). Dordrecht: Springer Netherlands. https://doi.org/10.1007/978-94-011-0249-0_2
- Liu, C., & Shan, Y. (2019). Analytical model for predicting the longitudinal profiles of velocities in a channel with a model vegetation patch. *Journal of Hydrology*, 576, 561–574. <https://doi.org/10.1016/j.jhydrol.2019.06.076>
- Liu, C., Shan, Y., Sun, W., Yan, C., & Yang, K. (2020). An open channel with an emergent vegetation patch: Predicting the longitudinal profiles of velocities based on exponential decay. *Journal of Hydrology*, 582, 124429. <https://doi.org/10.1016/j.jhydrol.2019.124429>
- Marjoribanks, T. I., Hardy, R. J., Lane, S. N., & Parsons, D. R. (2017). Does the canopy mixing layer model apply to highly flexible aquatic vegetation? Insights from numerical modelling. *Environmental Fluid Mechanics*, 17, 277–301. <https://doi.org/10.1007/s10652-016-9482-z>
- Montakhab, A., Yusuf, B., Ghazali, A. H., & Mohamed, T. A. (2012). Flow and sediment transport in vegetated waterways: A review. *Reviews in Environmental Science and Biotechnology*, 11, 275–287. <https://doi.org/10.1007/s11157-012-9266-y>
- Monti, A., Omidyeganeh, M., Eckhardt, B., & Pinelli, A. (2020). On the genesis of different regimes in canopy flows: A numerical investigation. *Journal of Fluid Mechanics*, 891. <https://doi.org/10.1017/jfm.2020.155>
- Murphy, E., Ghisalberti, M., & Nepf, H. M. (2007). Model and laboratory study of dispersion in flows with submerged vegetation. *Water Resources Research*, 43, 1–12. <https://doi.org/10.1029/2006WR005229>
- Naot, D., Nezu, I., & Nakagawa, H. (1996). Hydrodynamic behavior of partly vegetated open channels. *Journal of Hydraulic Engineering*, 122, 625–633. <https://doi.org/10.1061/ASCE/0733-9429>
- Nepf, H. M. (2012). Hydrodynamics of vegetated channels. *Journal of Hydraulic Research*, 50, 262–279. <https://doi.org/10.1080/00221686.2012.696559>
- Nezu, I., & Sanjou, M. (2008). Turbulence structure and coherent motion in vegetated canopy open-channel flows. *Journal of Hydro-Environment Research*, 2, 62–90. <https://doi.org/10.1016/j.jher.2008.05.003>
- Nikora, V. I., Cameron, S. M., Albayrak, I., Miler, O., Nikora, N., Siniscalchi, F., et al. (2012). Flow-biota interactions in aquatic systems: Scales, mechanisms, and challenges. In W. Rodi & M. Uhlmann (Eds.), *Environmental Fluid Mechanics: Memorial Volume in honour of Prof. Gerhard H. Jirka* (pp. 217–238). (IAHR Monographs). CRC Press/Balkema. <https://doi.org/10.1201/b12283>
- Okamoto, T. A., & Nezu, I. (2009). Turbulence structure and “Monami” phenomena in flexible vegetated open-channel flows. *Journal of Hydraulic Research*, 47, 798–810. <https://doi.org/10.3826/jhr.2009.3536>
- Pavlov, D. S., Mikheev, V. N., Lupandin, A. I., & Skorobogatov, M. A. (2008). Ecological and behavioural influences on juvenile fish migrations in regulated rivers: A review of experimental and field studies. *Hydrobiologia*, 609, 125–138. <https://doi.org/10.1007/s10750-008-9396-y>
- Poggi, D., Katul, G. G., & Albertson, J. D. (2004). A note on the contribution of dispersive fluxes to momentum transfer within canopies. *Boundary-Layer Meteorology*, 111, 615–621. <https://doi.org/10.1023/B:BOUN.0000016563.76874.47>
- Poggi, D., Porporato, A., Ridolfi, L., Albertson, J. D., & Katul, G. G. (2004). The effect of vegetation density on canopy sub-layer turbulence. *Boundary-Layer Meteorology*, 111, 565–587. <https://doi.org/10.1023/B:BOUN.0000016576.05621.73>
- Pope, S. B. (2000). *Turbulent flows*. Cambridge University Press. <https://doi.org/10.1017/CBO9780511840531>
- Prooijen, B. C., Van, Battjes, J. A., & Uijttewaal, W. S. J. (2005). Momentum exchange in straight uniform compound channel flow. *Journal of Hydraulic Engineering*, 131, 175–183. [https://doi.org/10.1061/\(ASCE\)0733-9429\(2005\)131](https://doi.org/10.1061/(ASCE)0733-9429(2005)131)
- Proust, S., Fernandes, J. N., Leal, J. B., Rivière, N., & Peltier, Y. (2017). Mixing layer and coherent structures in compound channel flows: Effects of transverse flow, velocity ratio, and vertical confinement. *Water Resources Research*, 53, 3387–3406. <https://doi.org/10.1002/2016WR019873>
- Raupach, M. R., Finnigan, J. J., & Brunet, Y. (1996). Coherent eddies and turbulence in vegetation canopies: The mixing-layer analogy. *Boundary-Layer Meteorology*, 78, 351–382. <https://doi.org/10.1007/BF00120941>
- Rogers, M. M., & Moser, R. D. (1994). Direct simulation of a self-similar turbulent mixing layer direct simulation of a self-similar turbulent mixing layer. *Physics of Fluids*, 6, 903–923.
- Rominger, J. T., & Nepf, H. M. (2011). Flow adjustment and interior flow associated with a rectangular porous obstruction. *Journal of Fluid Mechanics*, 680, 636–659. <https://doi.org/10.1017/jfm.2011.199>
- Roth, M., & Oke, T. R. (1995). Relative efficiencies of turbulent transfer of heat, mass, and momentum over a patchy urban surface. *Journal of the Atmospheric Sciences*, 52, 1863–1874.
- Rowiński, P. M., Västilä, K., Aberle, J., Järvelä, J., & Kalinowska, M. B. (2018). How vegetation can aid in coping with river management challenges: A brief review. *Ecohydrology and Hydrobiology*, 1–10, 345–354. <https://doi.org/10.1016/j.ecohyd.2018.07.003>
- Schnitzler, A., Hale, B. W., & Alsum, E. M. (2007). Examining native and exotic species diversity in European riparian forests. *Biological Conservation*, 138, 146–156. <https://doi.org/10.1016/j.biocon.2007.04.010>

- Siniscalchi, F., & Nikora, V. I. (2013). Dynamic reconfiguration of aquatic plants and its interrelations with upstream turbulence and drag forces. *Journal of Hydraulic Research*, *51*, 46–55. <https://doi.org/10.1080/00221686.2012.743486>
- Siniscalchi, F., Nikora, V. I., & Aberle, J. (2012). Plant patch hydrodynamics in streams: Mean flow, turbulence, and drag forces. *Water Resources Research*, *48*, 1–14. <https://doi.org/10.1029/2011WR011050>
- Sukhodolov, A. N., & Sukhodolova, T. A. (2012). Vegetated mixing layer around a finite-size patch of submerged plants: Part 2. Turbulence statistics and structures. *Water Resources Research*, *48*, 1–16. <https://doi.org/10.1029/2011WR011804>
- Tanino, Y., & Nepf, H. M. (2007). Experimental investigation of lateral dispersion in aquatic canopies. In 2007 IAHR congress proceedings. IAHR.
- Termini, D. (2015). Flexible vegetation behaviour and effects on flow conveyance: experimental observations. *International Journal of River Basin Management*, *13*, 401–411. <https://doi.org/10.1080/15715124.2015.1012519>
- Tinoco, R. O., San Juan, J. E., & Mullarney, J. C. (2020). Simplification bias: lessons from laboratory and field experiments on flow through aquatic vegetation. *Earth Surface Processes and Landforms*, *45*, 4743. <https://doi.org/10.1002/esp.4743>
- Truong, S. H., & Uijttewaal, W. S. J. (2018). Transverse momentum exchange induced by large coherent structures in a vegetated compound channel. *Water Resources Research*, *55*(1), 589–612. <https://doi.org/10.1029/2018WR023273>
- Västilä, K., & Järvelä, J. (2014). Modeling the flow resistance of woody vegetation using physically based properties of the foliage and stem. *Water Resources Research*, *50*, 229–245. <https://doi.org/10.1002/2013WR013819>
- Västilä, K., & Järvelä, J. (2018). Characterizing natural riparian vegetation for modeling of flow and suspended sediment transport. *Journal of Soils and Sediments*, *18*, 3114–3130. <https://doi.org/10.1007/s11368-017-1848-4>
- Västilä, K., Järvelä, J., & Aberle, J. (2013). Characteristic reference areas for estimating flow resistance of natural foliated vegetation. *Journal of Hydrology*, *492*, 49–60. <https://doi.org/10.1016/j.jhydrol.2013.04.015>
- Vogel, S. (1989). Drag and reconfiguration of broad leaves in high winds. *Journal of Experimental Botany*, *40*, 941–948. <https://doi.org/10.1093/jxb/40.8.941>
- Walling, D. E., Owens, P. N., Carter, J., Leeks, G. J. L., Lewis, S., Meharg, A. A., & Wright, J. (2003). Storage of sediment-associated nutrients and contaminants in river channel and floodplain systems. *Applied Geochemistry*, *18*, 195–220. [https://doi.org/10.1016/S0883-2927\(02\)00121-X](https://doi.org/10.1016/S0883-2927(02)00121-X)
- White, B. L., & Nepf, H. M. (2007). Shear instability and coherent structures in shallow flow adjacent to a porous layer. *Journal of Fluid Mechanics*, *593*, 1–32. <https://doi.org/10.1017/S0022112007008415>
- White, B. L., & Nepf, H. M. (2008). A vortex-based model of velocity and shear stress in a partially vegetated shallow channel. *Water Resources Research*, *44*, 1–15. <https://doi.org/10.1029/2006WR005651>
- Whittaker, P., Wilson, C. A. M. E., & Aberle, J. (2015). An improved Cauchy number approach for predicting the drag and reconfiguration of flexible vegetation. *Advances in Water Resources*, *83*, 28–35. <https://doi.org/10.1016/j.advwatres.2015.05.005>
- Wilson, C. A. M. E., Hoyt, J., & Schnauder, I. (2008). Impact of foliage on the drag force of vegetation in aquatic flows. *Journal of Hydraulic Engineering*, *134*, 885–891. <https://doi.org/10.1061/ASCE/0733-9429>
- Xiao, Y., Yang, Z., Wang, F., & Liu, M. (2020). Large eddy simulation of the hydrodynamic behavior of horizontal side jets in compound open channels with vegetated floodplain. *Environmental Science & Pollution Research*, *27*, 7967–7983. <https://doi.org/10.1007/s11356-019-07465-0>
- Xiaohui, S., & Li, C. W. (2002). Large eddy simulation of free surface turbulent flow in partly vegetated open channels. *International Journal for Numerical Methods in Fluids*, *39*, 919–938. <https://doi.org/10.1002/flid.352>
- Xu, Z. X., Ye, C., Zhang, Y. Y., Wang, X. K., & Yan, X. F. (2019). 2D numerical analysis of the influence of near-bank vegetation patches on the bed morphological adjustment. *Environmental Fluid Mechanics*, *20*, 707–738. <https://doi.org/10.1007/s10652-019-09718-5>
- Yan, C., Shan, Y., Sun, W., Liu, C., & Xingnian, L. (2020). Modeling the longitudinal profiles of streamwise velocity in an open channel with a model patch of vegetation. *Environmental Fluid Mechanics*, *20*, 1441–1462. <https://doi.org/10.1016/j.jhydrol.2019.124429>

References From the Supporting Information

- Andelin, M. (2019). *Development of experimental methods for investigating sediment and nutrient transport in vegetated flows* (Master thesis). Retrieved from Aalto University institutional online repository. Aalto University School of Engineering.
- Caroppi, G., Västilä, K., Gualtieri, P., Järvelä, J., Giugni, M., & Rowiński, P. M. (2020). *Acoustic Doppler Velocimetry (ADV) data on flow-vegetation interaction in partly vegetated channels with flexible and rigid vegetation*. Mendeley Data. Retrieved from <https://doi.org/10.17632/p6m666p4kb.1>
- Peltier, Y., Rivière, N., Proust, S., Mignot, E., Paquier, A., & Shiono, K. (2013). Estimation of the error on the mean velocity and on the Reynolds stress due to a misoriented ADV probe in the horizontal plane: Case of experiments in a compound open-channel. *Flow Measurement and Instrumentation*, *34*, 34–41. <https://doi.org/10.1016/j.flowmeasinst.2013.08.002>
- White, B. L., & Nepf, H. M. (2008). A vortex-based model of velocity and shear stress in a partially vegetated shallow channel. *Water Resources Research*, *44*, 1–15. <https://doi.org/10.1029/2006WR005651>
- Whittaker, P. (2014). *Modelling the hydrodynamic drag force of flexible riparian woodland* (Doctoral Dissertation). Cardiff University.